Electronic Supplementary Material (ESI) for Materials Chemistry Frontiers.

Molecular Layer-by-layer Re-stacking of MoS_2-In_2Se_3 by Electrostatic means: Assembly of a New Layered Photocatalyst

Bryan K Y Ng[1,‡], Cherie C Y Wong[1,‡], Wentian Niu[1], Hector P Garcia[2], Yiyang Li[1], Ping-Luen Ho[1], Winson C H Kuo[3], Robert A Taylor[4], Keita Taniya[5], Qi Wei[6], Mingjie Li[6], Michail Stamatakis[2,*], Shik Chi Edman Tsang[1,*]

[1]Wolfson Catalysis Centre, Department of Chemistry, University of Oxford, OX1 3QR, UK.
[2]Thomas Young Centre and Department of Chemical Engineering, University College London, Roberts Building, Torrington Place, London WC1E 7JE, UK

[3]Materials Characterization Facility, Texas A&M University, College Station, TX, 77843, USA

[4]Department of Physics, Clarendon Laboratory, Parks Road, Oxford, OX1 3PU, UK

[5]Department of Chemical Science and Engineering, Graduate School of Engineering, Kobe University, 1-1 Rokkodai, Nada, Kobe 657-8501, Hyogo, Japan

[6]Department of Applied Physics, The Hong Kong Polytechnic University, Hung Hom, Kowloon, Hong Kong, PR China

‡These authors contributed equally.

Corrsepondence to edman.tsang@chem.ox.ac.uk and m.stamatakis@ucl.ac.uk

Table of Contents

Experimental details

Chemicals

All chemicals and solvents in this work were commercially available, with 98 % purity or above, and used as received. In_2Se_3 (99.99%, metal basis, Alfa Aesar); MoS_2 powder (reagent grade, Sigma-Aldrich); n-butyllithium (1.6 M in hexanes, reagent grade, Sigma-Aldrich); Hexane (≥95%, HPLC, Sigma-Aldrich); Isopropanol (99.9%, Sigma-Aldrich); Hydrochloric acid (ACS reagent, 37%, Sigma-Aldrich); Thiourea (≥99.0%, ACS reagent, Sigma-Aldrich); Polyvinylpyrrolidone (PVP, average mol wt. 40,000, reagent grade, Sigma-Aldrich); Sodium hydroxide (≥97.0%, pellets, ACS reagent, Sigma-Aldrich); Argon gas (99.99%, BOC); Helium gas (99.99%, BOC); Nitrogen gas (99.99%, BOC).

Characterisation techniques

X-ray diffraction (XRD) measurement was performed using Bruker AXS D8 Advance ECO with LynxEye detector and Copper Kα radiation (λ = 1.5406 Å) with an energy of 8.04 keV. XRD patterns were collected scanning from 5° to 90° with a step size of 0.0195° and a step time of 0.100 s.

Atomic force microscopy (AFM) was performed by Bruker MM-8 High-resolution AFM with PeakForce Tapping Mode and SNL-10 cantilever, the voltage setpoint was 0.3 V to maintain constant height accuracy. The sample was dispersed in isopropanol and sonicated for 3 hours. Then, the solution was centrifuged at 1500 rpm for 5 minutes to remove large particles. The suspension (2.5 µL) was drop-casted on ultra-flat mica and dried at room temperature.

Atomic-resolution HAADF-STEM imaging with a probe current of 80 pA, and a semi-convergence angle of 23.6 mrad was performed at an accelerating voltage of 300 kV using an ThermoFisher Themis Z300 scanning transmission electron microscope equipped with a two-condenser-lens system, a monochromator unit and a CS probe corrector (CEOS). The microscope was aligned before every experiment by using a gold standard sample ensuring 0.06 nm resolution under normal conditions.

EDS elemental mapping was carried out from its highly sensitive Super-X energy dispersive x-ray spectrometer which contains a high-speed, high-throughput, quad-silicon drift detector optimized for rapid x-ray collection (0.9 srad) and when combined with STEM enables EDS spectral mapping down to the atomic scale. The microscope was set to C2 aperture at 70 µm with beam current was set between 150~200 pA during the EDS data acquisition. The dwell time was set to 100 µs per pixel with a map size of 256 × 256 pixels; a complete process of EDS mapping took roughly 1 h to reach an appropriately high signal-to-noise ratio. The catalyst suspensions were prepared by dispersing 1 mg of sample in approximately 1 mL of dry ethanol. The mixture was sonicated for 30 minutes to form a uniform suspension. The thin-film sample for TEM (less than 200 nm thick) was then prepared by the deposition of one drop of the as-prepared catalysis suspension onto a Holey carbon film 400 copper mesh grid and dried in the air prior to analysis. Finally, the copper sample grid was transferred to the sample holder of the TEM for measurements.

X-ray photoelectron spectroscopy (XPS) was performed using a Kratos Axis SUPRA XPS fitted with a monochromated Al K_a X-ray source (1486.7 eV), a spherical sector analyser and 3 multichannel resistive plates, 128 channel delay line detectors. All data was recorded at 150W and a spot size of 700 × 300 μm. Survey scans were recorded at pass energy of 160 eV, and high-resolution scans were recorded at pass energy of 20 eV. Electronic charge neutralization was achieved using a magnetic immersion lens. Filament current = 0.27 A, charge balance = 3.3 V, filament bias = 3.8 V. All sample data was recorded at a pressure below 10^{-8} Torr and a room temperature of 294 K. Data was analysed using CasaXPS v2.3.20PR1.0 and the spectra were calibrated with C 1s peak at 284.8 eV.

Ultraviolet photoelectron spectroscopy (UPS) was performed with He I at the energy of 21.2 eV.

Ultraviolet-visible diffuse reflectance spectroscopy (UV-Vis DRS) was performed using Shimadzu UV-2600 under diffuse reflectance mode. Barium sulphate pallet was used as the white diffuse standard.

Time-resolved photoluminescence (TRPL) spectroscopy was performed to measure the photoluminescence spectra and corresponding exciton lifetimes. A bespoke micro photoluminescence setup was used, in which a Ti-Sapphire laser (λ = 375 nm, pulse duration = 150 fs, repetition rate = 76 MHz) was directed onto the sample. Time-resolved measurements were performed using the spectrometer as a monochromator before passing the selected signal to a photomultiplier tube (PMT) detector with an instrument response function width of ~150 ps connected to a time-correlated single-photon counting module.

Continuous-wave electron paramagnetic resonance (CW EPR) spectroscopy was performed by an X-band (9.4 GHz) Bruker EMX EPR spectrometer. All EPR experiments were done at 293 K. 10 mg of sample was weighed and put into an EPR tube (0.60 i.d. and 0.84 o.d.). All X-Band spectra were collected over a 300 Gauss field range and 15 scans were adopted for the measurements.

Zeta potential measurement was performed by Malvern Zetasizer Nano ZS. The samples were dispersed in deionised water at pH 7 and at a temperature of 298 K. The Dispersant RI was 1.330, viscosity is 0.8872 cP and dispersant dielectric constant is 78.5.

Transient absorption spectroscopy was performed by using Helios pump/probe setup (Ultrafast Systems) with an amplified Ti: sapphire femtosecond laser (800 nm wavelength, 50 fs, 1 kHz repetition rate; Coherent Libra). The 400 nm pump pulses were obtained by frequency doubling the 800 nm fundamental regenerative amplifier output. The white light continuum probe pulses were generated by focusing a small portion of the regenerative amplifier's fundamental 800 nm laser pulses into a 2 mm sapphire crystal**.** The exciton lifetime is obtained by fitting the photo-induced absorption spectra with a mono-exponential decay function.

Evaluation of photocatalytic performance

The photocatalytic activity was mainly determined by the hydrogen evolution rate (μmol h^{-1} g^{-1}) from water splitting. The methodology of the testing is derived from the work from Li *et al.*[1]. Reactions were carried out in a closed 25 mL stainless steel autoclave system (Parr, United States) equipped with two quartz windows (with a diameter of 10 mm and a thickness of 18 mm). Control experiments reveal that no hydrogen was produced without catalyst and light irradiation under detection limit. In a typical activity test, 10 mg of catalyst was added to 8 mL Milli-Q H_2O in a quartz lining (20 mm i.d. × 24 mm o.d. × 52 mm height), then the autoclave was purged with 6 bar of Ar gas after being tightly sealed for 8 times. The mixture in the reactor would then be allowed to heat up to 270°C under vigorous magnetic stirring (750 rpm). Xenon lamp (300 W, Industrial Grade Arc Lamp with Dual Plano-Convex Lens, Fused Silica, Ozone-free, Newport) was then used to shine through the quartz windows at 10 cm. After 2 hours reaction, the autoclave was cooled down naturally to room temperature. The content of hydrogen was measured by gas chromatography (GC) equipped with thermal conductivity detectors (TCD) with He as the carrier gas, respectively. The calibration curves calculating the amount of hydrogen as follows. The percentage by volume of hydrogen is obtained by multiplying the area under the curve from the GC by 0.0016, derived from calibration curve.

Extended X-ray Absorption Fine Structure (EXAFS) measurement

X-ray absorption spectroscopy (XAS) data is measured at beamline BL02B1 of Spring8 in Japan. Transmission mode was used for all measurements and achieved by using a cylindrical imaging plate and photo-multiplier. The EXAFS data analysis was performed using IFEFFIT with Horae packages (Athena and Artemis)[2]. The fitting was done in R-space with k^3-weighted data. The amplitude reducing parameter was obtained from the literature of the corresponding element, which was used as a fixed input parameter in the data fitting to allow the refinement in the coordination number of the absorption element. The goodness of fit is evaluated by a low R-value.

Density Functional Theory (DFT) Calculations

Present details of the periodic DFT calculations follow the discussion in the main text. A dense Γ-centred k-point grid of $60/a \times 60/b \times 60/c$ was used, with non-integer values rounded up to the nearest integer. The effect of core electrons on the valence electron density was taken into account through the Projected Augmented Wave (PAW) method[3, 4]. Final total energies were obtained by extrapolation to 0 K (no smearing). Spin polarization was considered for all DFT calculations.

The bulk structures for 2H-MoS_2, S and Se were obtained from the Materials Project open dataset (mp-2815, mp-77 and mp-14, respectively), while the bulk structure for 2H-In_2Se_3 was built using VESTA software[5] based on the crystal structure data reported by Küpers et al[6]. The models for the MoS_2/In_2Se_3 monolayer stacking were constructed from the optimised bulk structures. Due to the different lattice parameters between MoS_2 and In_2Se_3 structures (i.e., 3.162 and 4.070 Å, respectively), 4×4 layers of MoS_2 were stacked on top of 3×3 layers of In_2Se_3, which match with around 3% difference. All possible stacking configurations were considered, leading to very similar

results. The S/Se mixed layer models were constructed by removing the top and bottom Se layers from In_2Se_3 and replacing some S atoms by Se. Different degrees of Se substitution into S were investigated, where 1, 2 or 4 S atoms for each S layer were replaced by Se, leading to 6.2%, 12.5% and 25% Se substitution (i.e., each S layer contains 16 atoms). For each %Se, 10 different models were created with randomly chosen substitutions.

The vacancy formation energy, E_f, was calculated as:

$$E_f = E_{sys-vac} - E_{sys} + \mu_i$$

where $E_{sys-vac}$ and E_{sys} are the total energies of the vacancy-containing and the stoichiometric configurations, respectively, and μ_i is the chemical potential of the atom i removed to generate the vacancy. In this work, μ_i is set as the energy per atom in the most stable bulk phase for i (μ_i≈($\mu_i \approx E_{bulk,i}/N_{bulk}$) where $E_{bulk,i}$ and N_{bulk} are the total energy and the number of atoms contained in the bulk unit cell. In order to minimize the impact of the vacancy on the charge distribution, large 5×5×2 and 4×4×2 supercells containing 300 and 320 atoms were used for MoS_2 and In_2Se_3, respectively, when computing $E_{sys-vac} - E_{sys}$.

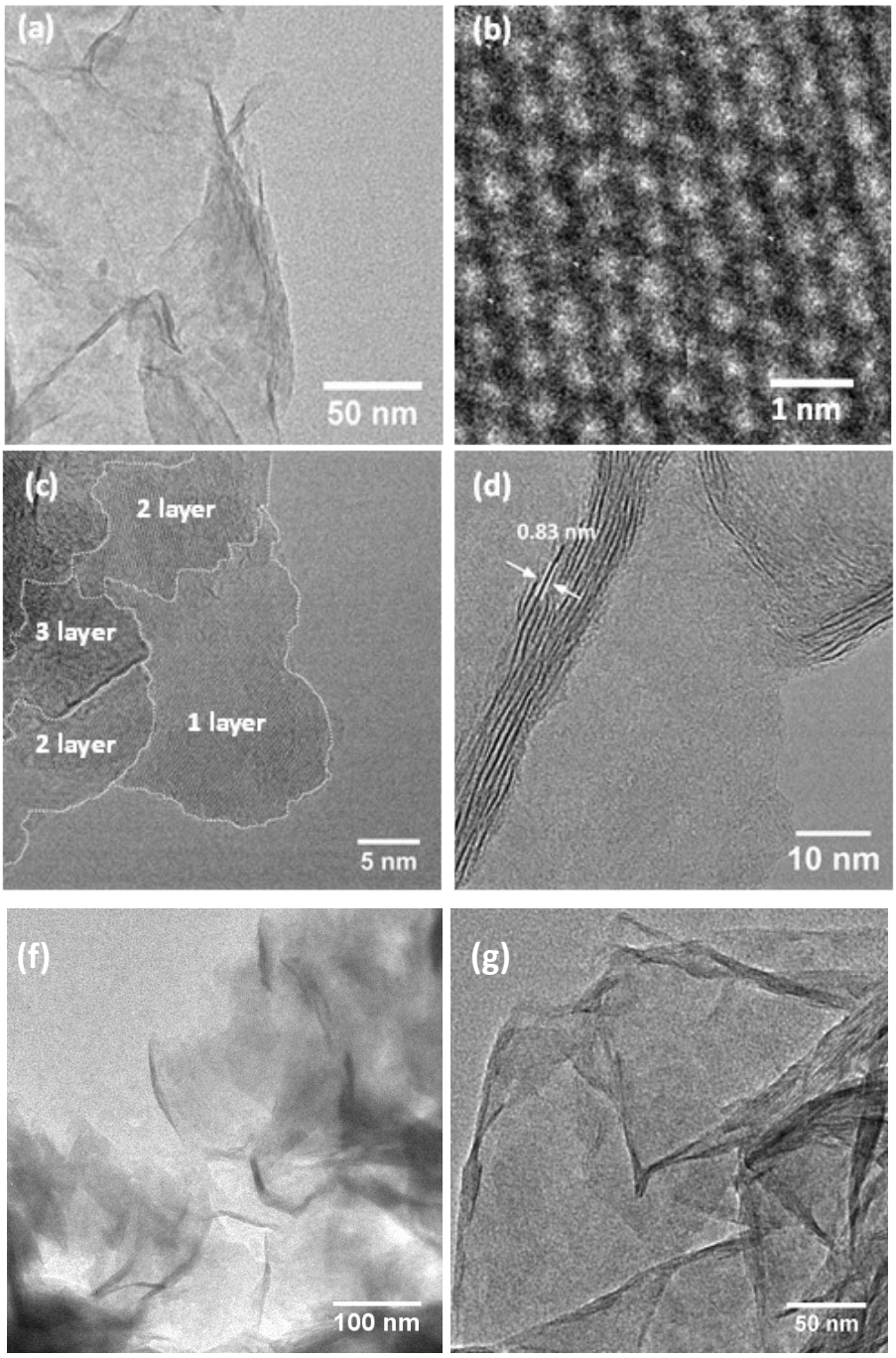
(a)
50 nm
(b)
1 nm
(c)
2 layer
3 layer
1 layer
2 layer
5 nm
(d)
0.83 nm
10 nm
(f)
100 nm
(g)
50 nm

Supplementary figure S1: a, Typical sheet- like morphology exfoliated metal chalcogenide from bulk using Li treatment-sonication. HRTEM images of **b,** typical structure of the MoS_2. **c,** Top view and **d,** side view of restacked region of MoS_2. While minor agglomeration and restacking was taken place, most areas of ex-MoS_2 as seen from images **f** and **g** still show a sheet-like morphology.

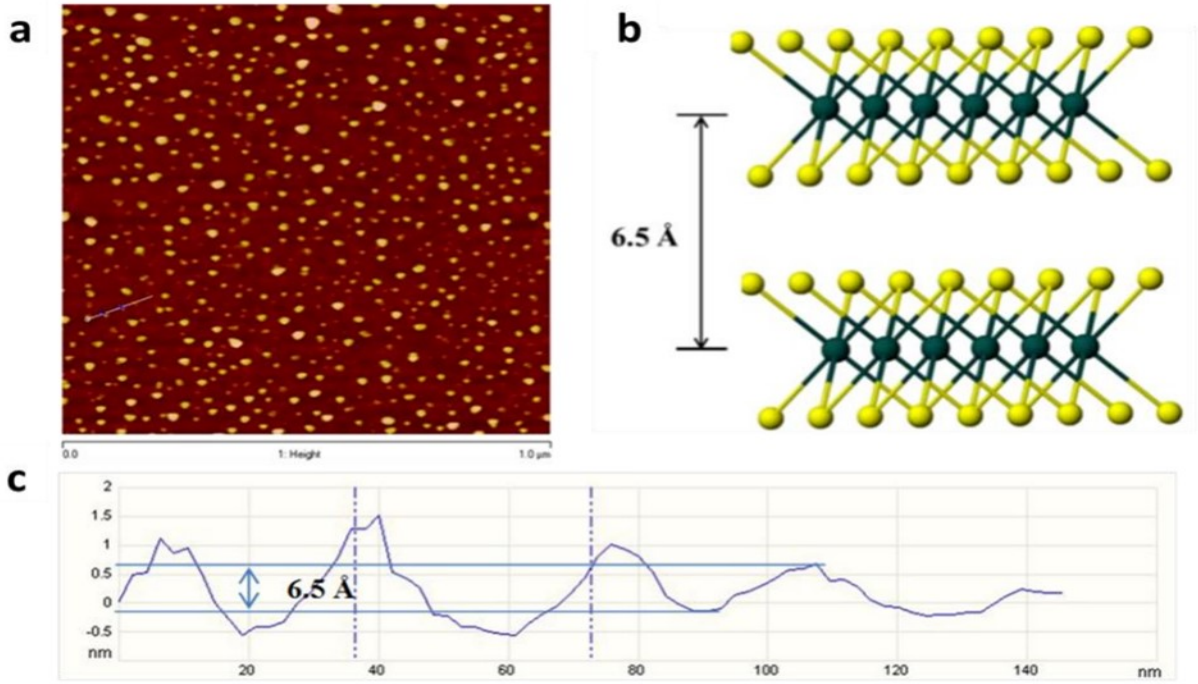

Supplementary figure S2: **a**, typical AFM image of exfoliated MoS_2. **b**, ideal structure of 2H-MoS_2 before exfoliation. **c**, height profile corresponding to the blue line, pointed out by a white arrow, on the AFM image. The lateral dimension of the exfoliated MoS_2 ranges from 20-40 nm, and has step heights of approximately 6-10Å. This value is comparable to the 6.5Å distance separating between the two layers in the bulk 2H-MoS_2 structure. The average topographic height is around 1.04 nm, which correlates well with the height of monolayer MoS_2 with adsorbed water molecules[7].

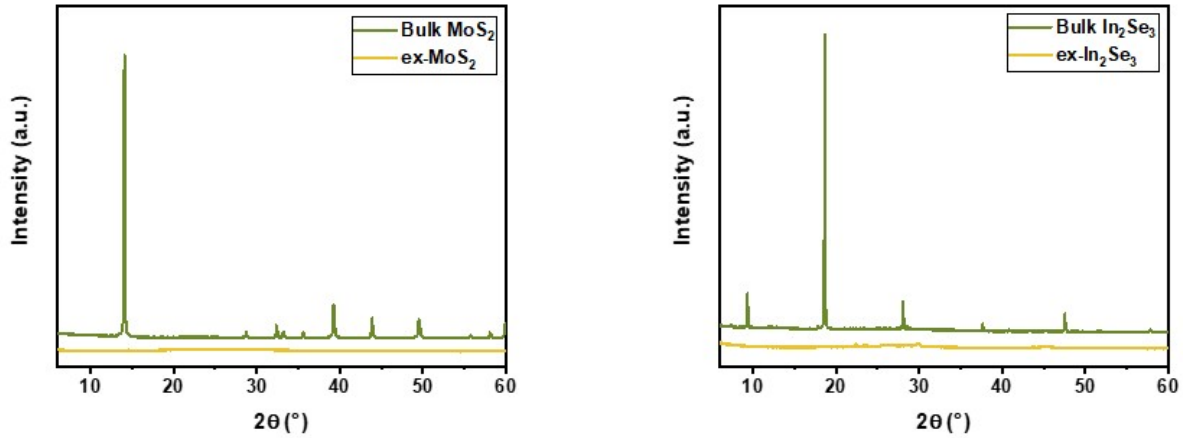

Supplementary figure S3: Typical XRD pattern of bulk MoS_2 and ex-MoS_2 (left); XRD pattern of bulk In_2Se_3 and exfoliated ex-In_2Se_3 (right).

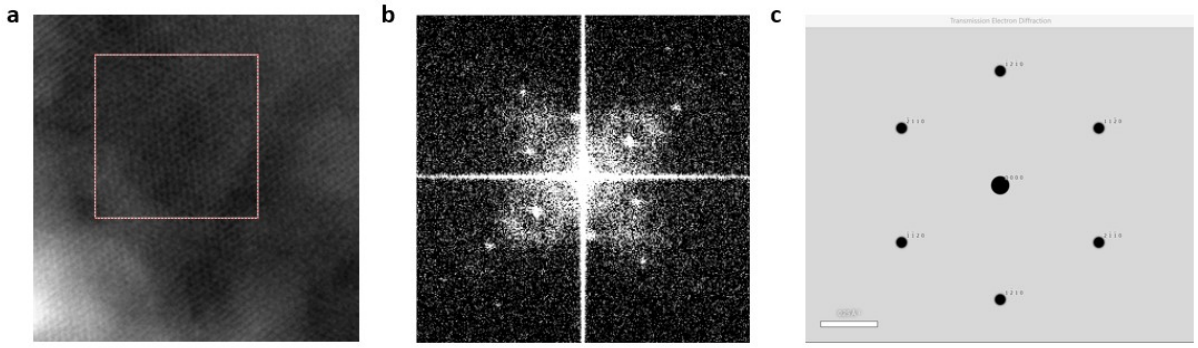

Supplementary figure S4. **a**, TEM image and its fast fourier transform (**b**). **c**, simulated diffraction pattern of bulk α-In_2Se_3.

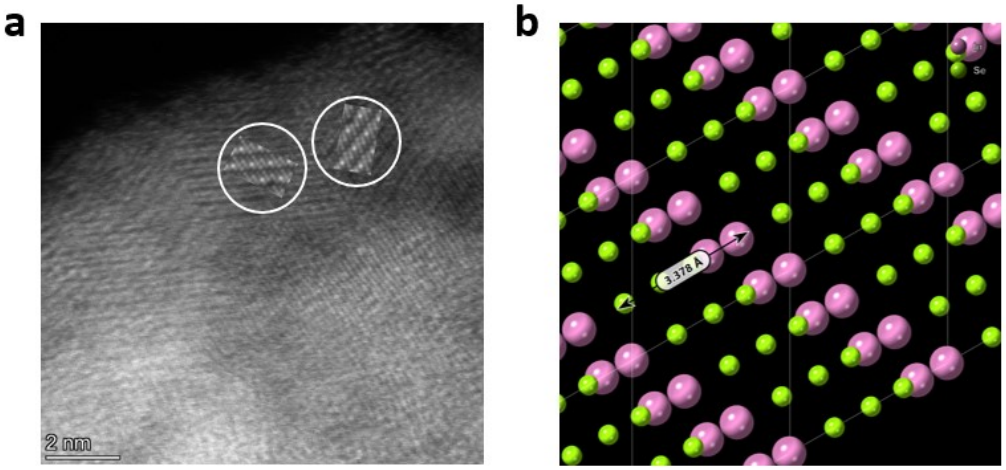

Supplementary figure S5: **a**, HAADF-STEM image of bulk α-In_2Se_3, with patches of simulated image laid on top of the experimental image. **b**, Atomic model which

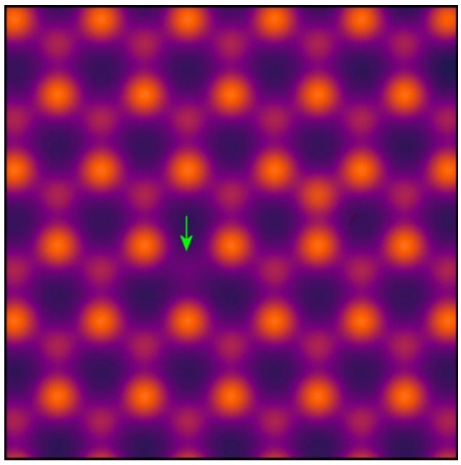

generated the simulated image.

Supplementary figure S6: HADDF-STEM image simulation of Supplementary figure S1b. Green arrow shows a single S vacancy in single layer MoS_2[8].

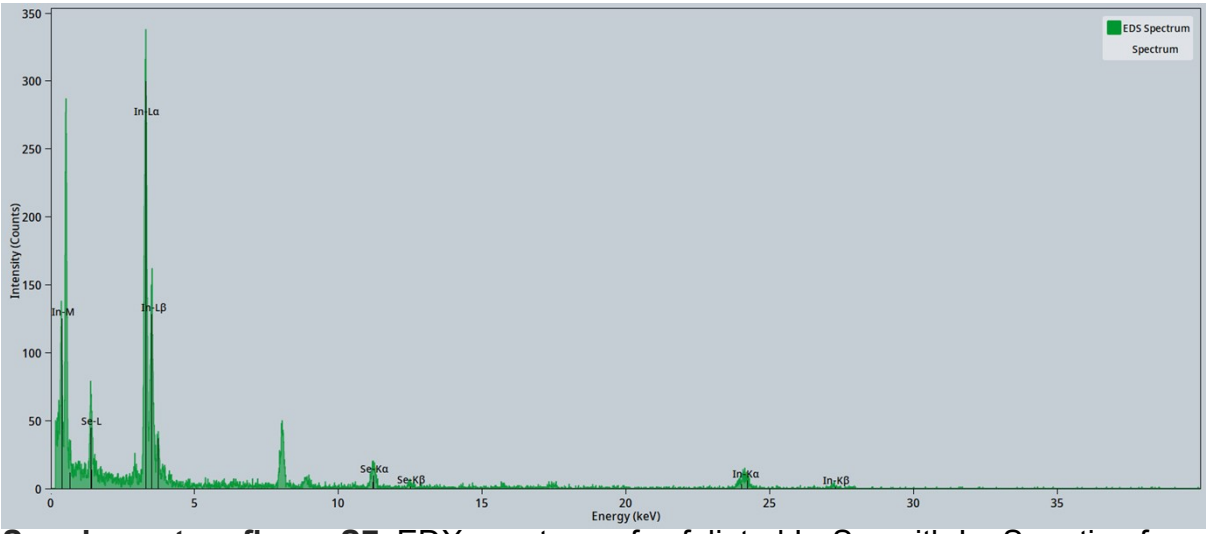

Supplementary figure S7: EDX spectrum of exfoliated In_2Se_3 with In: Se ratio of 87:13, which is significantly deviated to the expected ratio of 2:3 in bulk In_2Se_3, with the EDX results summarised in Table 1.

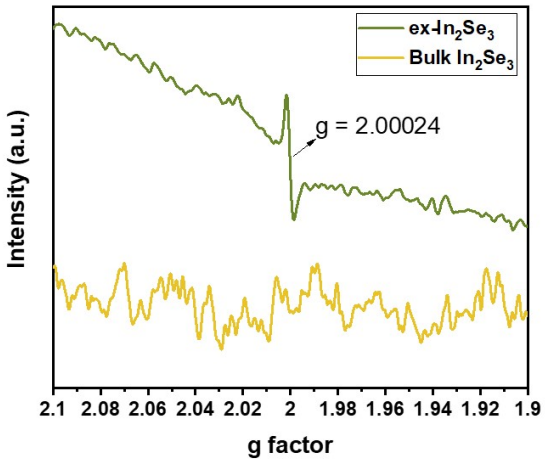

Supplementary figure S8: EPR spectra of exfoliated In_2Se_3 and Bulk In_2Se_3

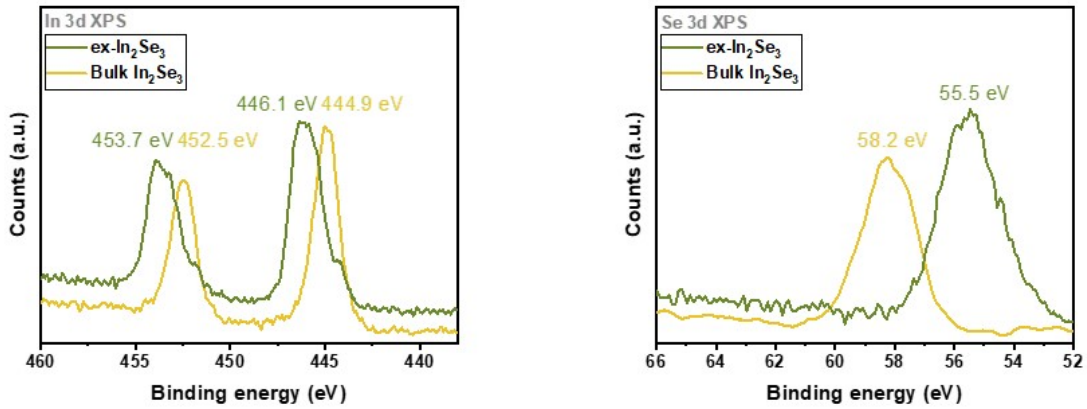

Supplementary figure S9: **a**, In 3d XPS of ex-In_2Se_3 and bulk In_2Se_3. **b**, Se 3d XPS of ex-In_2Se_3 and bulk In_2Se_3

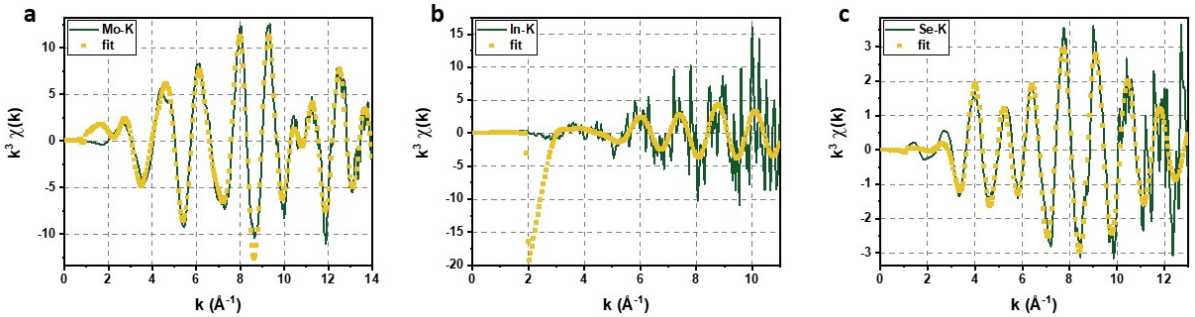

Supplementary figure S10: Mo K-edge (**a**), In K-edge (**b**) and Se K-edge (**c**) k^3-weighted k-space EXAFS spectra for MoS_2-In_2Se_3 multi-heterojunction

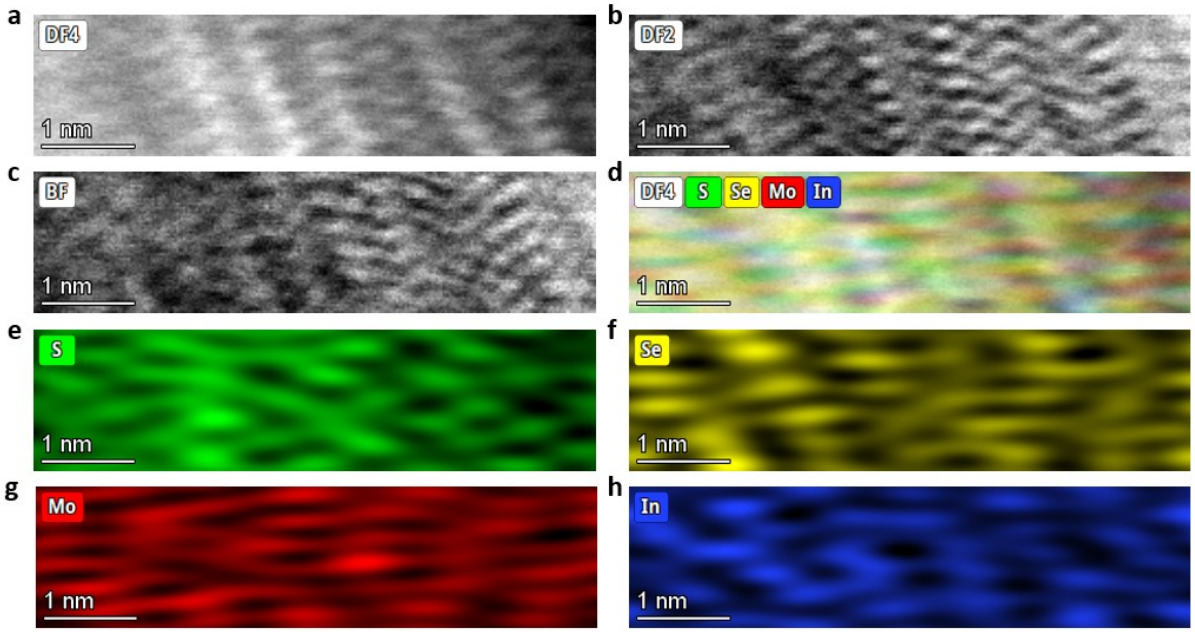

Supplementary figure S11: Atomic pattern and Super EDX of near MoS_2- In_2Se_3 surface under dark field (**a,b**), bright field (**c**), and its combined EDX mapping (**d**). The individual atomic EDX mapping of S(**e**), Se(**f**), Mo(**g**) and In(**h**).

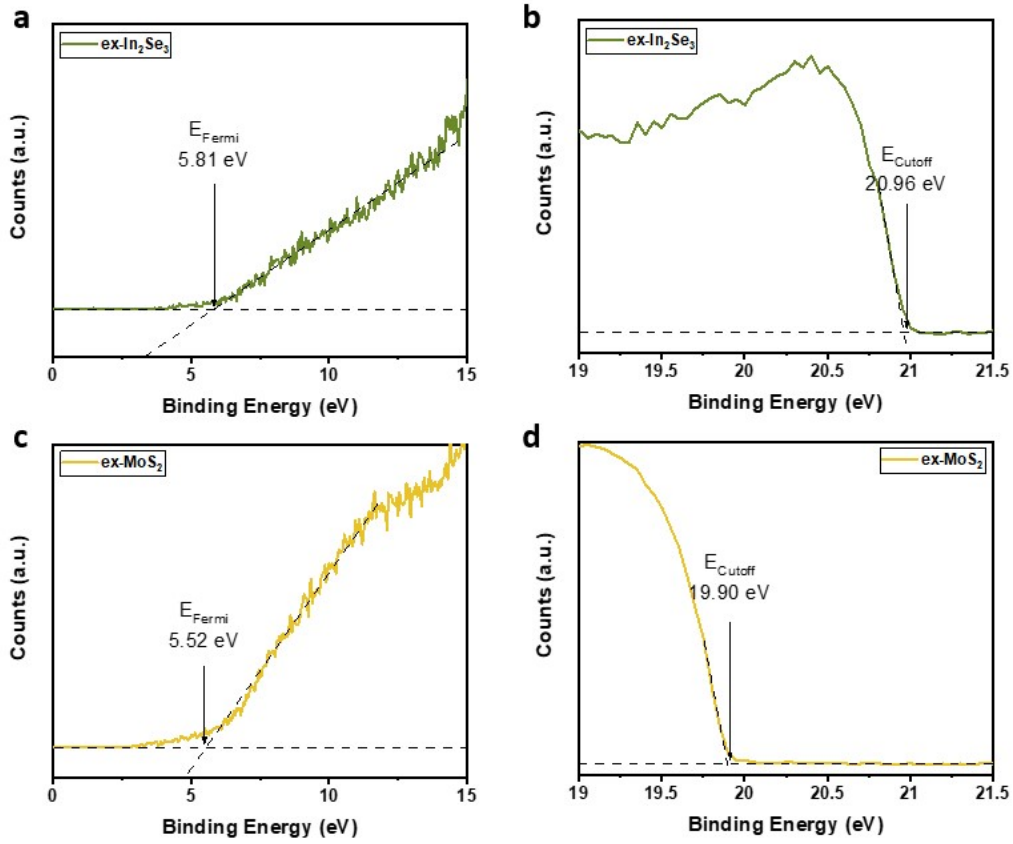

Supplementary figure S12: **a**, Fermi energy and **b**, Cutoff energy of ex-In_2Se_3 obtained from UPS spectra. **c**, Fermi energy and **d**, Cutoff energy of ex-MoS_2 obtained from UPS spectra.

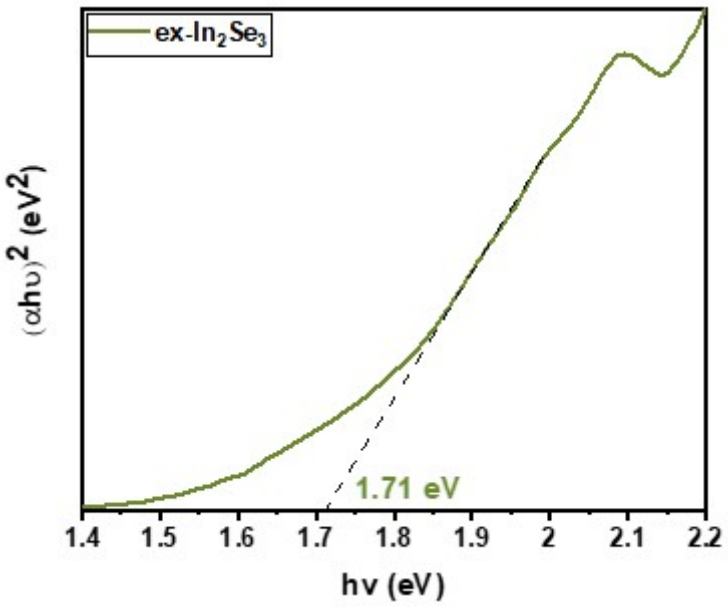

Supplementary figure S13: **a**, Tauc plot of ex-In_2Se_3, with band gap energy taken to be 1.71 eV. The bandgap energy of ex-MoS_2 is taken from Ryon et. al. to be 1.86 eV[9].

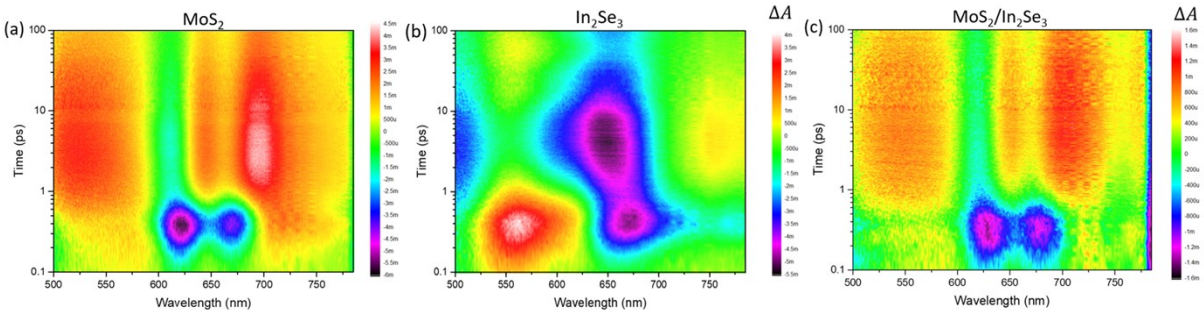

Supplementary figure S14: Pseudocolor TAS data of ex-MoS_2(**a**), ex-In_2Se_3(**b**) and MoS_2-In_2Se_3 (**c**) heterojunction excited by 400 nm fs laser with pump fluence of 6 μJ cm^{-2}.

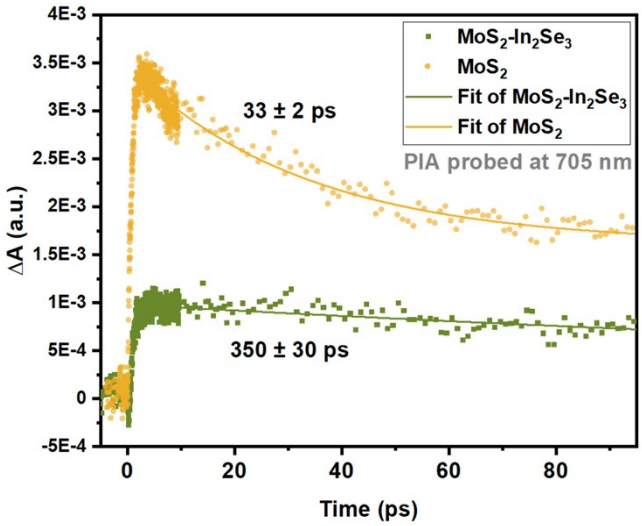

Supplementary figure S15: PIA dynamics probed at 705nm for ex-MoS_2 compared to MoS_2-In_2Se_3. Lifetime with error is obtained by fitting data to a single-exponential decay function.

Z	Element	Family	Atomic fraction (%)	Atomic error (%)	Mass fraction (%)	Mass error (%)	Fit error (%)
34	Se	K	13.28	1.75	9.52	1.31	2.22
49	In	K	86.72	1.75	90.48	1.31	4.33

Z	Element	Family	Atomic fraction (%)	Atomic error (%)	Mass fraction (%)	Mass error (%)	Fit error (%)
34	Se	L	13.66	1.44	9.81	1.08	1.67
49	In	L	86.34	1.44	90.19	1.08	0.21

Supplementary table 1: EDX results (K and L emission lines) of ex-In_2Se_3

Sample	Zeta potential (mV)
ex-In_2Se_3	+ 27.6 ± 3.88
ex-MoS_2	- 34.4 ± 7.79

Supplementary table 2: Zeta potential of ex-In_2Se_3 and ex-MoS_2

Path	CN	R / Å	D-W factor / 10^{-3}
Mo-S	5.60 ± 0.20	2.40 ± 0.01	3.4 ± 0.9
Mo-Se	0.34 ± 0.13	2.60 ± 0.04	3.4 ± 0.9
Mo-Mo	5.06 ± 0.30	3.17 ± 0.01	5.5 ± 1.2
Mo-In	0.28 ± 0.53	3.97 ± 0.12	5.5 ± 1.2
		$S_0^2 = 0.90$[10]	R = 1.53%
Fitting space: Δk 2-14 ΔR 1-4	Background removal: E_0(all) = 20005.4 eV		

Supplementary table S3a: EXAFS fitting parameters of Mo K-edge of MoS_2-In_2Se_3 multi-heterojunction

Path	CN	R / Å	D-W factor / 10^{-3}
In-Se	2.85 ± 0.21	2.66 ± 0.07	5.6 ± 1.5
In-S	1.15 ± 0.21	3.02 ± 0.06	5.6 ± 1.5
		$S_0^2 = 0.95$[11]	R = 4.66%
Fitting space: Δk 3-11 ΔR 1.7-3.3	Background removal: E_0(S) = 27940.1 eV	Background removal: E_0(Se) = 27953.1 eV	

Supplementary table S3b: EXAFS fitting parameters of In K-edge of MoS_2-In_2Se_3 multi-heterojunction

Path	CN	R / Å	D-W factor / 10^{-3}
Se-In	1.93 ± 0.73	2.60 ± 0.02	10.6 ± 3.6
Se-Mo	2.23 ± 1.27	2.61 ± 0.04	12.9 ± 8.9
		S_0^2 = 0.90[12]	R = 0.74%
Fitting space: Δk 2-12 ΔR 1.3-3	Background removal: R_{bkg}=1.25 Å	Background removal: E_0(In) = 12661.7 eV	Background removal: E_0(Mo) = 12650.7 eV

Supplementary table S3c: EXAFS fitting parameters of Se K-edge of MoS_2-In_2Se_3 multi-heterojunction

System	Vacancy	Formation energy (eV)
2H-MoS_2	S	2.86
	Mo	7.25
2H-In_2Se_3	Se	0.53
	In	3.90
Stacked MoS_2-In_2Se_3	S	2.79
	Se	1.14

Supplementary table S4: Vacancy formation energy of S, Se, Mo and In in bulk In_2Se_3, bulk MoS_2 and stacked MoS_2-In_2Se_3

References

1. Li Y, Wu S, Zheng J, Peng Y-K, Prabhakaran D, Taylor RA*, et al.* 2D photocatalysts with tuneable supports for enhanced photocatalytic water splitting. *Materials Today* 2020, **41:** 34-43.

2. Ravel B, Newville M. ATHENA, ARTEMIS, HEPHAESTUS: data analysis for X-ray absorption spectroscopy using IFEFFIT. *J Synchrotron Radiat* 2005, **12**(Pt 4)**:** 537-541.

3. Blochl PE. Projector augmented-wave method. *Phys Rev B Condens Matter* 1994, **50**(24)**:** 17953-17979.

4. G. Kresse DJ. From ultrasoft pseudopotentials to the projector augmented-wave method. *Physical Review B* 1999, **59:** 1758.

5. Momma K, Izumi F. VESTA 3for three-dimensional visualization of crystal, volumetric and morphology data. *Journal of Applied Crystallography* 2011, **44**(6)**:** 1272-1276.

6. Kupers M, Konze PM, Meledin A, Mayer J, Englert U, Wuttig M*, et al.* Controlled Crystal Growth of Indium Selenide, In2Se3, and the Crystal Structures of alpha-In2Se3. *Inorg Chem* 2018, **57**(18)**:** 11775-11781.

7. Jia T, Li MM, Ye L, Wiseman S, Liu G, Qu J*, et al.* The remarkable activity and stability of a dye-sensitized single molecular layer MoS2 ensemble for photocatalytic hydrogen production. *Chem Commun (Camb)* 2015, **51**(70)**:** 13496-13499.

8. Lau THM, Lu X, Kulhavy J, Wu S, Lu L, Wu TS*, et al.* Transition metal atom doping of the basal plane of MoS2 monolayer nanosheets for electrochemical hydrogen evolution. *Chem Sci* 2018, **9**(21)**:** 4769-4776.

9. Ryou J, Kim YS, Kc S, Cho K. Monolayer MoS2 Bandgap Modulation by Dielectric Environments and Tunable Bandgap Transistors. *Sci Rep* 2016, **6:** 29184.

10. Wang-Jae Chun KA, Yasuhiro Iwasawa*. Polarization-Dependent Total-Reflection Fluorescence XAFS Study of Mo Oxides on a Rutile TiO2(110) Single Crystal Surface. *J Phys Chem B* 1998, **102:** 9006-9014.

11. Narita H, Tanaka M, Shiwaku H, Okamoto Y, Suzuki S, Ikeda-Ohno A*, et al.* Structural properties of the inner coordination sphere of indium chloride complexes in organic and aqueous solutions. *Dalton Trans* 2014, **43**(4)**:** 1630-1635.

12. Pietnoczka A, Bacewicz R, Antonowicz J, Schorr S, Gurieva G. EXAFS Study of the Local Order in Cu2ZnSn(SxSe1-x)4 Alloys. *physica status solidi (b)* 2019, **256**(11).